nature communications

Article

https://doi.org/10.1038/s41467-025-58147-0

An epidermal serine sensing system for skin healthcare

Received: 14 September 2024

Accepted: 10 March 2025

Published online: 18 March 2025

Check for updates

Ying Yuan[1,2,3,4], Bowen Zhong[1,2,4], Xiaokun Qin[1,2], Hao Xu[1,2] ✉, Zhexin Li[1,2], Linlin Li[1,2], Xiaofeng Wang[1,2], Wenxuan Zhang[1,2], Zheng Lou[1,2] ✉, Yongming Fan[3] ✉ & Lili Wang[1,2] ✉

Portable biosensors mainly focus on detecting biomarkers in biofluids but neglect the abundant skin biomarkers on the stratum corneum, which are associated with the functionality and integrity of the skin barrier. Here, we propose a sensing patch designed for direct sampling and in situ quantification of epidermal serine, an important biomarker for skin healthcare. The patch consists of a porous hydrogel for serine diffusion and ion conduction, and a molecular imprinted polymer-based electrochemical serine sensor. By integrating with a customized handheld serine tester, the serine sensing system enables in situ measurement of epidermal serine levels. We demonstrate the application of this serine sensing system in assessing the moisturizing effect of a skincare product and tracking the recovery progress of skin barrier function in a patient with atopic dermatitis. Our work opens up a potential application scenario for portable biosensors in personalized skin healthcare.

With the rapid advancements in biosensing technology, portable or wearable biosensors have emerged as a research frontier due to their unique advantages, demonstrating immense potential in monitoring human physiological processes and disease states[1,2]. Portable biosensors have aimed to detect biomarkers in biofluids, such as sweat[3], saliva[4], tears[5], and interstitial fluid[6]. Among them, sweat contains abundant biomarkers such as amino acids[7], lactic acid[8], electrolytes[9], proteins[10], and even steroid hormones[11], which can be continuously and non-invasively collected and detected. These characteristics make it one of the research hotspots of portable biosensors[12]. In general, traditional sweat induction requires additional and active sweat generation methods, including physical exertion, heat, and iontophoresis[13,14], which may cause user exhaustive even discomfort, as well as potential side effects for patients[15]. Recently, passive sweat generation methods have emerged and are attractive for their convenience against active methods[16,17]. Leveraging diffusion extraction, a variety of hydrogel-based sensors have been developed to sample and detect passive sweat biomarkers generated by natural perspiration and reside on the skin surface[18,19]. However, apart from sweat biomarkers on the skin, the epidermis also contains a large number of intrinsic biomarkers stem from skin metabolism[20], which play an important role in the skin barrier while have not yet been reported on portable biosensors.

Such epidermal biomarkers refer to solid-phase skin metabolic products residing on the skin surface or within the stratum corneum, which can reflect the integrity of the skin barrier and are thus widely tested in dermatology as well as cosmetics[21]. Compared to biomarkers in biofluids, epidermal biomarkers persistently presented on the skin can be non-invasively and user-friendly determined without the need for any biofluid generation methods[22]. These epidermal biomarkers have opened up avenues for early diagnosis and treatment of various skin diseases, particularly for those intimately linked to skin barrier function, such as atopic dermatitis (AD)[23]. However, the direct extraction and the in-situ detection of epidermal biomarkers still confront numerous challenges. First, for the extraction, traditional skin sampling methods often involve invasive or minimally invasive procedures, including skin biopsy or tape stripping, which are laborious, poorly tolerated by patients, and may lead to

[1]State Key Laboratory of Semiconductor Physics and Chip Technologies, Institute of Semiconductors, Chinese Academy of Sciences, Beijing, China. [2]Center of Materials Science and Optoelectronic Engineering, University of Chinese Academy of Sciences, Beijing, China. [3]Key Laboratory of Lignocellulosic Chemistry, College of Material Science and Technology, Beijing Forestry University, Beijing, China. [4]These authors contributed equally: Ying Yuan, Bowen Zhong. ✉e-mail: haoxu19@semi.ac.cn; zlou@semi.ac.cn; fanym@bjfu.edu.cn; liliwang@semi.ac.cn

local trauma or infection[24]. Existing reported non-invasive sampling techniques address some of the issues inherent in invasive skin sampling, but they usually necessitate further sample processing steps (e.g., extraction, purification, and pre-concentration) before metabolite detection[25,26]. This not only escalates testing cost and time but also potentially affects the accuracy and reliability of results. Second, for the detection, common measurement technologies, including liquid chromatography-mass spectrometry (LC-MS)[27] and enzyme-linked immunosorbent assay (ELISA)[28], are limited by their disadvantages like cumbersome instrumentation, time-consuming and labor-intensive professional operation. Therefore, there remains an urgent need for a universal technique to achieve direct sampling and in-situ measurement of epidermal metabolites. In theory, the passive diffusion sampling method and the wearable electrochemical detection technique can meet the above need but have not yet been demonstrated for sensing epidermal biomarkers.

Within the realm of epidermal biomarkers, natural moisturizing factors (NMF) have garnered considerable attention due to their crucial physiological roles in the skin's chemical barrier. NMF is a mixture of small biological molecules produced in the stratum corneum, such as pyrrolidone carboxylic acid, amino acids, urea, lactates, etc[29]. Variations in NMF levels directly correlate with changes in the functionality and integrity of the skin barrier[30,31]. Therefore, NMF has found applications in the assessment of skin barrier impairment and disruption, as well as the identification and prediction of certain skin diseases, such as AD[32]. Notably, serine is the most abundant amino acid in NMF (accounting for over one-fifth of total free amino acids in NMF)[33], which plays a pivotal role in skin hydration due to its high concentration and remarkable water retention[34]. Furthermore, serine possesses multiple barrier functions as follows: (1) extracellular lipid biosynthesis for the maintenance of skin structure[35]; (2) Immune response support for skin inflammation[36]; (3) keratinocyte turnover for the exfoliation and renewal of the stratum corneum[37]. Given the high proportion of serine in NMF and its pivotal role in skin hydration and barrier function, the level of epidermal serine is considered a significant biochemical indicator to evaluate skin health[38,39]. Specifically, the determination of serine content in the stratum corneum provides a valuable reference for dermatologists to assess the severity of skin barrier-related diseases, including psoriasis[40], AD[41], and xerosis[42]. Furthermore, serine also plays a key role in various cellular and neural functions. Therefore, dysregulation of serine metabolism is also associated with a variety of health conditions beyond skin health, such as neurological disorders (schizophrenia, amyotrophic lateral sclerosis, epilepsy), cancer, metabolic disorders, and immune dysfunctions[43,44]. The critical health roles of serine metabolism highlight the importance of monitoring serine levels, particularly in non-invasive assessment of serine content on the epidermis for skin healthcare.

In this article, we develop a wearable serine sensing patch designed for direct sampling and in situ detection of epidermal serine (Fig. 1a). This disposable and low-cost patch comprises two key components: (1) a highly porous and permeable polyvinyl alcohol (PVA) hydrogel serving as the serine diffusion and ion-conductive layer; (2) a serine sensor based on the molecular imprinted polymer (MIP) for highly selective capture and sensitively detection of serine sampled by the hydrogel. When coupled with a customized serine electrochemical tester, this integrated serine sensing system enables the real-time measurement and readout of epidermal serine levels, and thus reliably evaluates the integrity of the skin barrier. Users can be easily informed of their skin health status by using our integrated serine sensing system, and its simple and efficient operation is comparable to commercially available glucose meters. By tracking changes in epidermal serine levels on the skin, we successfully demonstrated the system application for the enhanced moisturizing function of the skin after subjects applied a specific commercial skin essence. Moreover, we also continuously monitored the treatment and recovery process of skin barrier function in an AD patient after using a prescription drug. These results indicate that our epidermal serine sensing system is amenable for applications in the effectiveness assessment of skincare products in cosmetics and the management of chronic skin diseases in dermatology.

Results

Design and operation of the epidermal serine sensing system

As the key unit of the epidermal serine sensing system, the serine sensor (Fig. 1a) is primarily comprised of two essential components: a porous PVA hydrogel for serine diffusion and ion conduction, and a MIP-based electrochemical electrode array for serine sensing. Furthermore, the serine sensor was packaged as a wearable patch (Fig. 1a), which consists of a sensing chamber made of a double side tape to place the PVA hydrogel and define the sensing area, as well as top and bottom encapsulation layers made of waterproof tapes to prevent the moisture evaporation from the hydrogel. The laser cutting technique was employed to fabricate the structural shape of serine sensors and the packaging materials of patches, which are mass-producible and low-cost (Supplementary Fig. 1).

Notably, unlike the existing structure for passive sweat sampling, the serine sensing patch adopts a structure with three separate banded three electrodes sandwiched between the hydrogel and the skin (Fig. 1a–c). Compared with the structure of the hydrogel sandwiched between a whole electrode substrate and the skin, the separate electrodes are easier to bend and deform than the whole electrode plate, so that the hydrogel, the electrodes, and the skin contact each other more closely. Moreover, the contact area between the hydrogel and the skin is relatively small due to the exitance of the separate electrodes in the middle, which reduces the potential skin irritation to the diseased skin from the salt solution in the hydrogel.

When the patch intimately adheres to the skin surface, a concentration gradient is established between the serine-free hydrogel and the serine-rich skin through the gaps between the electrodes. This serine concentration gradient drives the diffusion of serine from the stratum corneum wetted by the hydrogel towards the patch. During this process, the water-soluble serine molecules traverse the intercellular space or cell membranes of the stratum corneum and subsequently diffuse into the hydrogel matrix and the electrode surface (Fig. 1b). After that, the carbon electrodes with a serine-imprinted polymer layer specifically recognize the serine molecules in the hydrogel matrix. Finally, the electrode array transduces serine-MIP bindings into an electrochemical signal through an ionic conduction pathway after the serine concentration distribution reaches a quasi-steady state (Fig. 1c). This selective binding between serine and the MIP layer reduces the contact between the redox probe layer and the electrolyte solution, thereby hindering the electron transfer process[45] (Fig. 1c).

By developing a handheld and portable electrochemical tester, the integrated serine sensing system achieved the non-invasive and in situ detection of epidermal serine (Supplementary Fig. 2–4). To demonstrate its practical application value in skin diseases, we employed the serine sensing system to effectively distinguish between the skin lesions and nearby normal areas for an AD patient, and continuously track the treatment and recovery process during three consecutive weeks of topical medication (Fig. 1d). Our results uncover the disorder of skin serine metabolism during the pathological process of AD, and indicate that our system can offer a perspective for skin chronic inflammatory disease diagnosis, monitoring, and therapeutic assessment (Fig. 1d).

The operation steps of the serine sensing system are simple and convenient for users or patients (Fig. 1e and Supplementary Movie 1). The whole operation can be summarized by five steps: (1) Preparation: switch on the tester and prepare the encapsulated patch; (2) Calibration: Insert the patch into the tester and calibrate through the blank

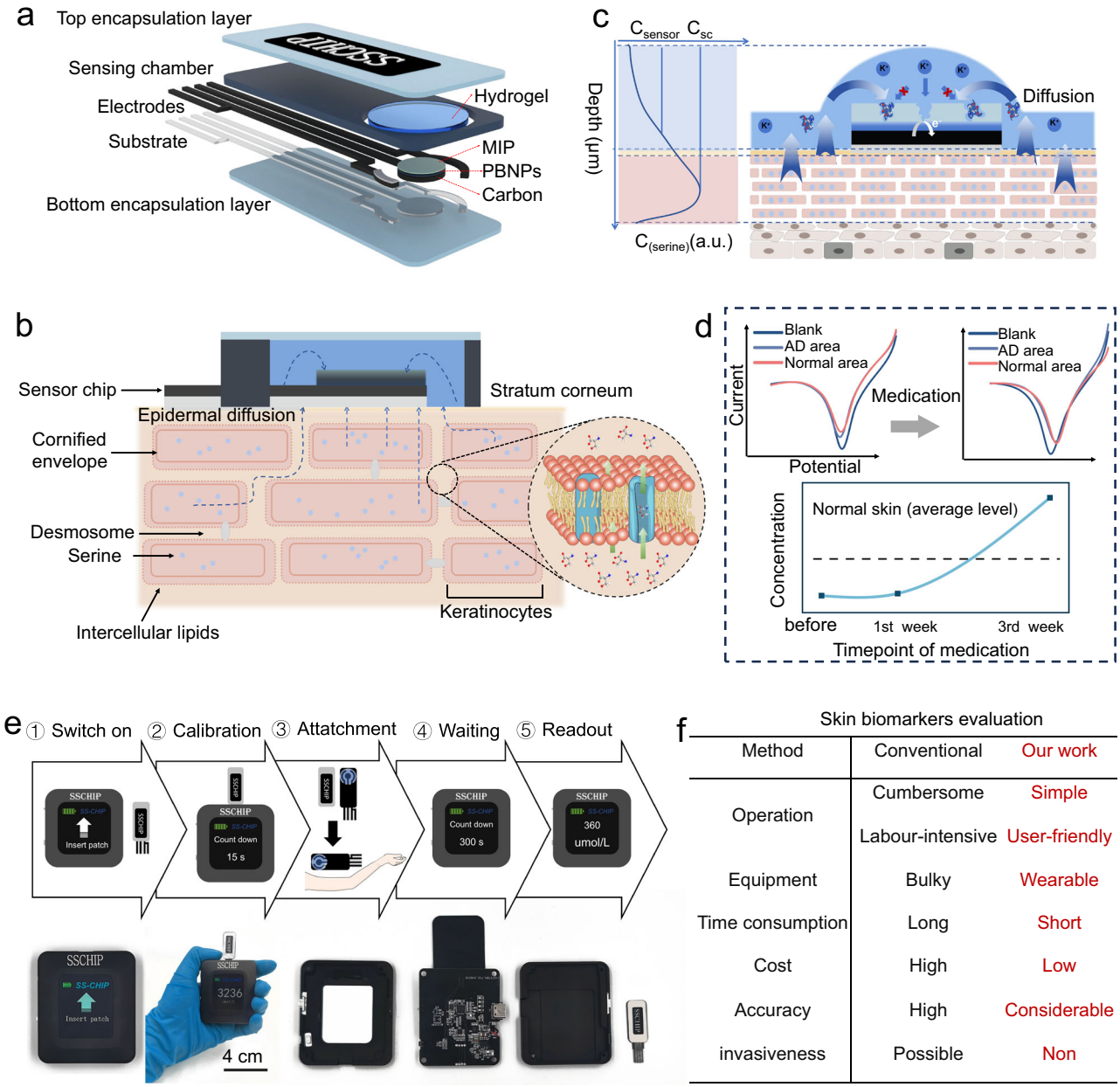

Method	Conventional	Our work
Operation	Cumbersome	Simple
	Labour-intensive	User-friendly
Equipment	Bulky	Wearable
Time consumption	Long	Short
Cost	High	Low
Accuracy	High	Considerable
invasiveness	Possible	Non

Fig. 1 | Design and operation of the epidermal serine sensing system. **a** Schematic of the wearable serine sensing patch. **b** Dissolution and diffusion process of epidermal serine after the patch attachment to the skin. The inset shows the serine leaving keratinocytes by passive transport. **c** Schematic diagram of serine measurement by the serine sensor in the hydrogel matrix, the left illustration shows the concentration distribution of serine in the stratum corneum and hydrogel. **d** Comparison of serine levels in the lesion area and normal area of an AD patient before and after three weeks of topical medication treatment. **e** Operation steps of the serine sensing system for epidermal serine detection and construction of the customized handheld serine tester consisting of an internal main control board, a display screen, a patch port, a rechargeable lithium battery, and buttons. **f** Comparison between the serine sensing system proposed in this article and traditional methods for skin biomarkers evaluation.

condition due to the variability between disposable patches; (3) Attachment: Peel off the top encapsulation layer of the patch and attach it on the skin to be tested; (4) Waiting: Waiting 5 minutes for the serine diffusion to a quasi-steady state; (5) Readout: Remove the patch from the skin, cover the top encapsulation layer, reinsert it into the tester again for the serine measurement, and read the result on the tester's display (Supplementary Fig. 4). Compared to the conventional measurement method for the skin biomarker, our serine sensing system offers remarkable advantages in several key aspects (Fig. 1f). This serine sensing system enables users to conduct self-monitoring at home or in a non-clinical setting, which significantly enhances treatment flexibility and patient engagement.

Characterization of MIP-based serine sensors

The electrochemical sensing electrode relies on the serine-imprinted polymer method for the indirect detection of non-electroactive serine molecules. Although many MIP-based sensors have been developed for the detection of amino acids in portable biosensors[46,47], the MIP-based serine sensor has not yet been demonstrated in epidermal serine detection because of its disregarded skin health significance by researchers[48]. In our design, to achieve high-performance serine sensing, a multi-layer sensitive and selective working electrode was prepared based on a spin-coated carbon conductive substrate, an electrodeposited Prussian blue nanoparticles (PBNPs) layer, and an electropolymerized serine-imprinted pyrrole layer (Fig. 2a). The

https://doi.org/10.1038/s41467-025-58147-0

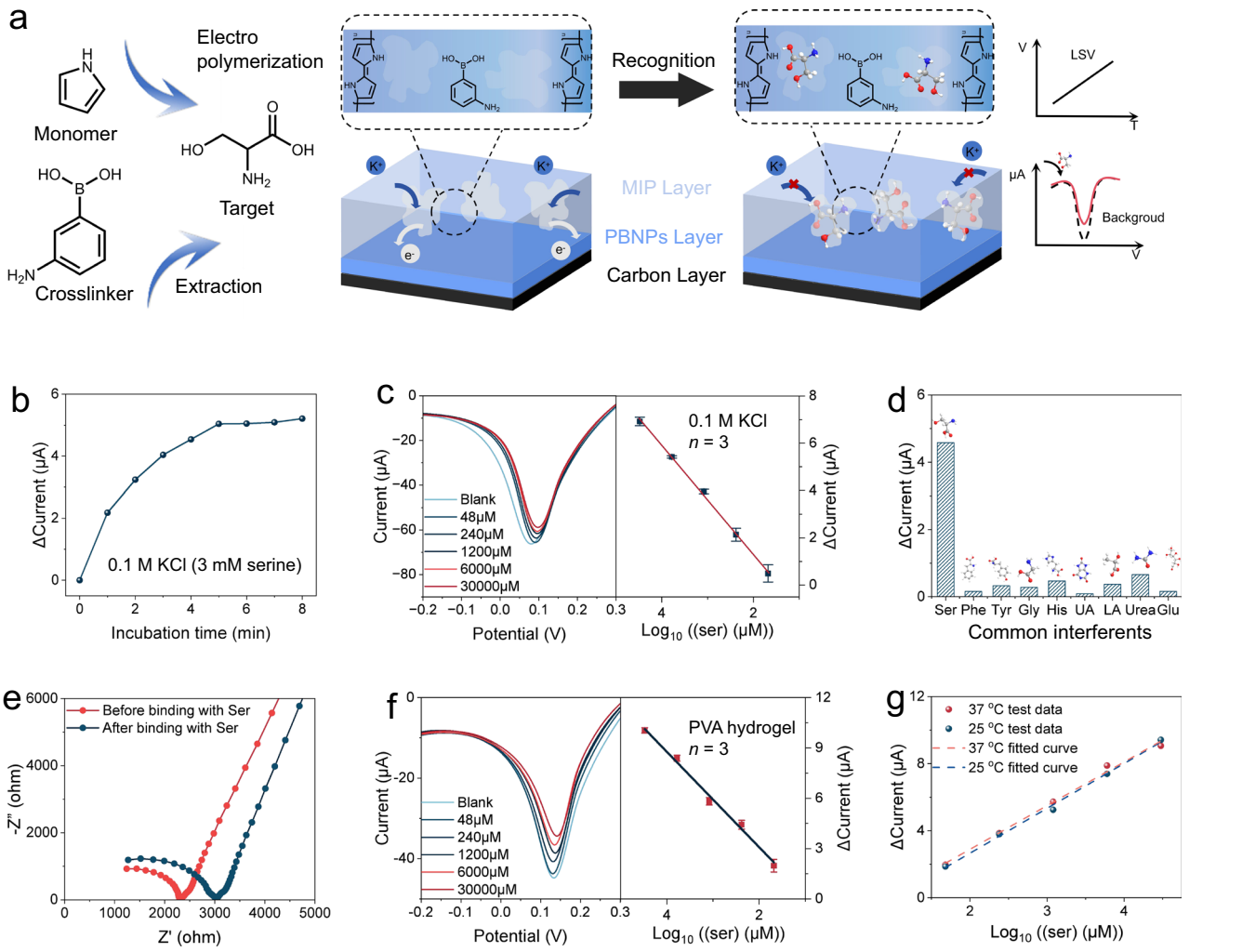

Fig. 2 | Characterization of MIP-Based Serine Sensors. a Synthesis and detection mechanism of the MIP-based serine sensor. **b** Optimization of the incubation time prior to serine sensing in 0.1 M KCl. 5 minutes of incubation was determined to be the most efficient and accurate incubation time for the serine to interact with the MIP electrode. **c** Electrochemical response of the MIP sensor to different serine concentrations in 0.1 M KCl and the corresponding calibration plot. The line represents the fitted trendline. Data are presented as mean values ± standard deviation (SD) from three electrodes. **d** Responses of the MIP serine sensor to different epidermal analytes (including phenylalanine, tyrosine, glycine, histidine, uric acid, lactic acid, glucose, and urea). The serine sensor shows insignificant response to these analytes, while it shows a clear response after the addition of serine. **e** EIS responses of a MIP-based electrode before and after binding with serine. **f** Electrochemical responses of the serine sensing patch to different serine concentrations in the porous PVA hydrogel containing 0.1 M KCl, and the corresponding calibration plot. The line represents the fitted trendline. Data are presented as mean values ± SD from three electrodes. **g** Responses of the serine sensing patch to different serine concentrations at different temperatures (25 °C and 37 °C) in porous PVA hydrogel containing 0.1 M KCl.

carbon electrode provides a stable, low-cost, and mass-fabricated conductive pathway and substrate for subsequent electrochemical steps (Supplementary Fig. 5). Within a specific potential window, the PBNPs layer undergoes reversible redox reactions and generates measurable current signals which provide the electrochemical signal basis for the serine detection of the working electrode. Meanwhile, the MIP layer further endows the working electrode with the selective ability for serine by simulating the function of bioaffinity antibodies.

To construct the MIP layer, pyrrole, 3-aminophenylboronic acid (APBA), and serine were selected as the functional monomer, the cross-linker, and the template, respectively. By removing the template molecules through subsequent solvent extraction steps, the produced cavities in the MIP layer not only match the spatial configuration of the template molecules, but also retain multiple interaction sites for the capture and recognition of serine molecules. When serine molecules specifically bind to the MIP layer, the contact area between the PBNPs layer and the electrolyte solution decreases. Consequently, during the detection of the reduction peak of Prussian blue via the linear sweep voltammetry (LSV) technique, the peak current density decreases progressively with the increases of serine concentrations (Fig. 2a). The serine level under the test condition can be obtained by the difference of the peak current density from the blank background solution (Supplementary Fig. 6). Detailed characterization, validation, and optimization of the MIP-based serine sensor are provided in Supplementary Notes 1 and 2 and Supplementary Fig. 7–9.

The interaction between serine and the MIP sensing electrode was investigated in a 0.1 M KCl solution. To study the time to reach sufficient and steady binding, the response signal intensity was recorded at various incubation time points. The current response decreases and eventually reaches a quasi-steady state at 5 minutes over time (Fig. 2b and Supplementary Fig. 10). Figure 2c demonstrates the sensor's wide detection range for serine (48 μM to 30 mM), where a logarithmic linear relationship exists between the decrease in peak current and serine concentration, with a sensitivity of 2.22 μA per decade of concentration. Furthermore, the MIP-based serine sensor exhibits excellent selectivity towards other non-target analytes (predominantly

water-soluble small molecules) present in the epidermis (Fig. 2d and Supplementary Fig. 11). Apart from the high sensitivity and selectivity in performance, the MIP-based serine sensor also shows good repeatability, stability and reproducibility (Supplementary Note 3, Figs. 12–15), which are necessary for the disposable use of the sensor.

In order to emulate the practical application environment, the MIP-based serine sensor was further characterized and evaluated in the porous PVA hydrogel for serine diffusion and detection. The thickness of the hydrogel is an important factor that directly affects the extraction efficiency and detection reliability for serine sensing. Therefore, we conducted the finite element simulations for thickness optimization (Supplementary Note 4 and Fig. 16). Numerical simulation results indicated that as the thickness of the hydrogel increased, serine molecules diffusing in the hydrogel matrix required a longer time to reach a quasi-steady state. Meanwhile, considering the limited water content and susceptibility to water loss in thin hydrogels (Supplementary Fig. 17), we determined 0.3 mm as the optimal thickness of the PVA hydrogel for detecting serine on the skin. After thickness optimization, the dried hydrogels respectively imbibed 30 μL of 0.1 M KCl solution to ensure the same moisture content, the diameter of the hydrogels after swelling was 9 mm. These hydrogels were then placed over the electrode surface and were conformal with the electrode due to their flexibility and gravity. Electrochemical impedance spectroscopy (EIS) provided further insights into the electron transfer mechanism at the hydrogel/electrode interface (Fig. 2e). The specific binding of serine molecules to the MIP layer on the electrode surface leads to an increase in the charge transfer resistance. This alteration manifests as an enlargement of the semicircle diameter in the high-frequency region of the Nyquist plot after serine binding (Fig. 2e).

In the ionic solution environment of the hydrogel matrix, the reduction peak current response (Fig. 2f) and the incubation time (Supplementary Fig. 18) of the MIP-based serine sensor on the integrated patch are similar to those in 0.1 M KCl solution. Specifically, within the detection range of 48 μM to 30 mM, the response current decreases with the increase of serine concentration in the hydrogel. The resulting decrease in peak current response depended logarithmically on the serine concentration with a sensitivity of 2.85 μA per decade of concentration. Based on this patch structure, the diffusion-current response behaviors in hydrogels with different thicknesses were measured on the skin of a subject (Supplementary Fig. 19). The experimental results of the time to reach the quasi-steady state at different thicknesses are consistent with the previous simulation results. Additionally, the serine sensing patch showed good current response stability across the skin temperature range (Fig. 2g).

After the serine sensor was packaged as the wearable patch, the stable sensing performance of the patch allows it to be stored in the air for at least 4 days (Supplementary Fig. 20). During measurement, users need to attach the wearable patch to their tested skin for at least 5 minutes to obtain a stable result, when the diffusion of serine in the hydrogel reaches a steady state (Supplementary Fig. 21).

System evaluation on skin moisturizing function

Cosmetic science studies have demonstrated a close correlation between the NMF content in the stratum corneum and skin moisturizing function[49]. Topical application of cosmetics containing NMFs can improve stratum corneum hydration and maintain skin barrier function[50]. To assess the skin moisturizing function and the efficacy of cosmetic products, existing portable devices almost rely on the measurement of physical indicators[51] and lack the ability to access molecular-level biochemical indicator information. Moreover, traditional techniques for skin biomarker sampling and detection cannot meet the need for in situ rapid analysis in non-clinical settings. In this regard, our portable serine sensing system with the wearable serine sensing patch achieved in situ measurement of the skin biomarker, serine. After the system measurement, the respective hydrogels from the patches used by eight subjects were collected to measure the average serine levels with a standard colorimetric assay kit. The linear relationship between the serine levels measured by the serine sensing system and the colorimetric results verified the measurement reliability of our system (Fig. 3a).

We conducted the following study to demonstrate its application for the efficacy evaluation of cosmetic products in improving the skin moisturizing function. A commercially available skin care product (L'Oréal Black Essence) containing moisturizing ingredients (including serine) for skin care was applied to the subject's skin surface where the serine levels were measured by our system before and after application (Fig. 3b). The skin of a subject's forearm was divided into two distinct areas—the blank skin and the moisturized skin. The moisturized skin refers to the skin where the essence was applied, while the blank skin refers to the unapplied skin. The measurements were repeated six times at adjacent locations within the two skin areas of the subject's forearm to verify the repeatability of the serine sensing system (Supplementary Fig. 22a). Before measuring serine levels, two crucial and complementary physical indicators, namely transepidermal water loss (TEWL) and stratum corneum hydration (SCH), were also recorded by a commercial portable instrument (GPSkin Barrier®) to evaluate the reliability of serine measurement. The coefficients of variation (CVs) in the measurements of our serine sensing systems on the two skin areas are 24.62% and 12.07%, respectively. These relatively large variations may be attributed to the inherent differences between adjacent skin locations in epidermal serine levels, rather than differences in our devices with acceptable repeatability and reliability. Furthermore, the average serine levels and SCHs on the moisturized skin area were both higher than those on the blank skin area, while TEWLs were reduced after skin moisturization (Fig. 3b and Supplementary Table 1). The results of these measurements and comparisons supported our hypothesis that the application of serine-rich essence can enhance the skin hydration and barrier function.

Users can independently perform epidermal serine measurement according to simple instructions and read the results on the tester (Fig. 3c and Supplementary Movie 1). In addition, TEWLs were also recorded in different subjects. After applying the essence to the subjects' inner forearm for 2 h, the peak current density detected by our system significantly decreased, corresponding to an increase in the serine content on the epidermis (Supplementary Fig. 23). For all subjects, serine levels were significantly higher on the skin with essence than on the adjacent skin without essence (Fig. 3d). This significant change before and after essence application ($^{**}P < 0.01$) was also statistically verified by a two-tailed paired *t*-test (Fig. 3e). Moreover, we uncovered that epidermal serine levels showed strong negative correlations with TEWL (Fig. 3f). Therefore, it can be inferred that the essence's moisturizing ingredients, including serine, remain in the stratum corneum after application and thus improve the skin hydration function, which was reflected in the increase of SCH and the decrease of TEWL (Fig. 3b). Meanwhile, by comparing the optical photos before and after applying essence, it can be found that the skin after applying essence become shinier (Supplementary Fig. 24).

The epidermal serine sensing system was also used to study the long-term moisturizing effect of the skin essence. The left inner forearm of a subject was divided into several areas where the essence was evenly extended proper amount and the patch was attached to measure epidermal serine levels at different time points. This method is to prevent artificially low serine levels caused by repeated samplings and measurements in the same area. After the essence application, the epidermal serine level rapidly elevated and reached the peak within 2 h after application. Although the serine level began to reduce due to the net consumption of serine in the stratum corneum over time, it still remained at a relatively high level compared to that of the skin before application (Supplementary Fig. 25). This changing trend agrees with that of the average total free amino acids

https://doi.org/10.1038/s41467-025-58147-0

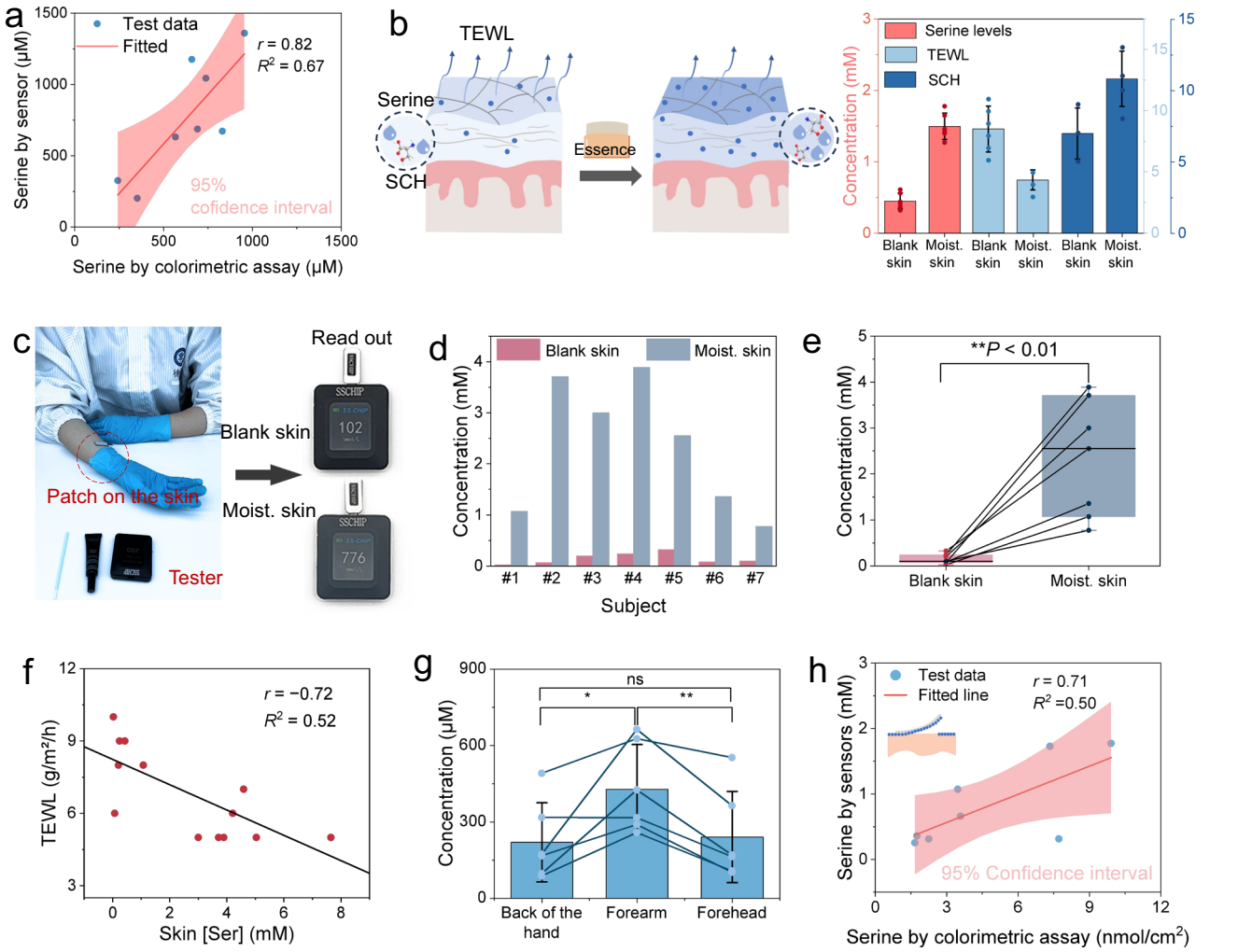

Fig. 3 | Serine sensing system for assessing moisturizing effect of skincare products. a Sensor-measured serine levels versus corresponding standard readouts in their hydrogels by a commercial serine colorimetric assay kit ($n = 8$ subjects). Pearson correlation coefficient, $r = 0.82$, Coefficient of determination, $R^2 = 0.67$. **b** Serine levels, SCHs, and TEWLs of the forearm skin of a subject moisturized with and without essence application (Blank skin and Moisturized skin). Six measurements were conducted using the serine sensing system and GPSkin Barrier® for repeatability verification. SCH and TEWL units are '%' and 'g/m²/h', respectively. Data are presented as mean values ± SD. **c** Photographs of a subject wearing the serine sensing patch on the left inner forearm. Detection results display on the handheld serine tester screen before and after essence application. **d** Changes in epidermal serine levels in 7 subjects after applying the essence. **e** Corresponding box-and-whisker plot of epidermal serine levels before and after essence application ($n = 7$). The difference is statistically significant (**$P < 0.01$, $P = 0.003$). The box ends represent the 25th and 75th percentiles. The horizontal line represents the median. The upper and lower whiskers represent the maxima and minima, respectively. **f** Correlation of sensor-measured serine levels and TEWLs obtained by the commercial instrument. $r = -0.72$. $R^2 = 0.52$. **g** Sensor-measured serine levels across different body parts ($n = 6$ subjects). The differences in epidermal serine levels are statistically significant between the forearm and forehead (**$P < 0.01$, $P = 0.002$), and between the forearm and back of hand (*$P < 0.05$, $P = 0.033$), but not statistically significant (ns) between the back of hand and forehead ($P > 0.05$, $P = 0.682$). Data are presented as mean values ± SD. **h** Sensor-measured serine levels versus corresponding standard readouts in the tape-stripping samples by the commercial serine colorimetric assay kit ($n = 8$ locations). $r = 0.71$. $R^2 = 0.50$. Inset: the schematic diagram of the tape-stripping method. All statistical analyses were performed using two-tailed paired t-tests. Lines in a, f, and h represent fitted trendlines.

(AAs) levels of the skin measured by a standard colorimetric assay in the retained hydrogel.

In addition, we measured the epidermal serine levels on different body parts of subjects to demonstrate the robustness of our serine sensing system. The measured results revealed the variations in serine content across different body parts as well as different individuals. Specifically, the serine levels in the inner forearm were higher than those on the forehead and back of the hand (Fig. 3g). The serine content in all three body parts showed a strongly positive correlation with the SCH values. However, these correlations varied across the different body parts due to the differences in the slopes of their fitted lines (Supplementary Fig. 26), which are consistent with the previously reported work[52]. Finally, to evaluate the accuracy of our device more precisely, we performed an additional standard validation using the tape stripping method, which is a widely recognized method for skin metabolomics studies. The experiment setup for this validation (Supplementary Fig. 22b) is similar to the above repeatability measurement experiment. Moreover, two tape-stripping samples from the forehead and the back of the hand of an identical subject in Fig. 3g were also collected for this validation. The serine levels in tape stripping samples determined by the commercial colorimetric assay kit are regarded as the serine levels in the stratum corneum of the subjects' skin. Our analysis revealed a linear relationship with a high correlation coefficient (r) of 0.71 ($n = 8$) between the serine levels measured by our serine sensing systems and the standard method (Fig. 3h, Supplementary Fig. 27, and Supplementary Table 2). In summary, all above

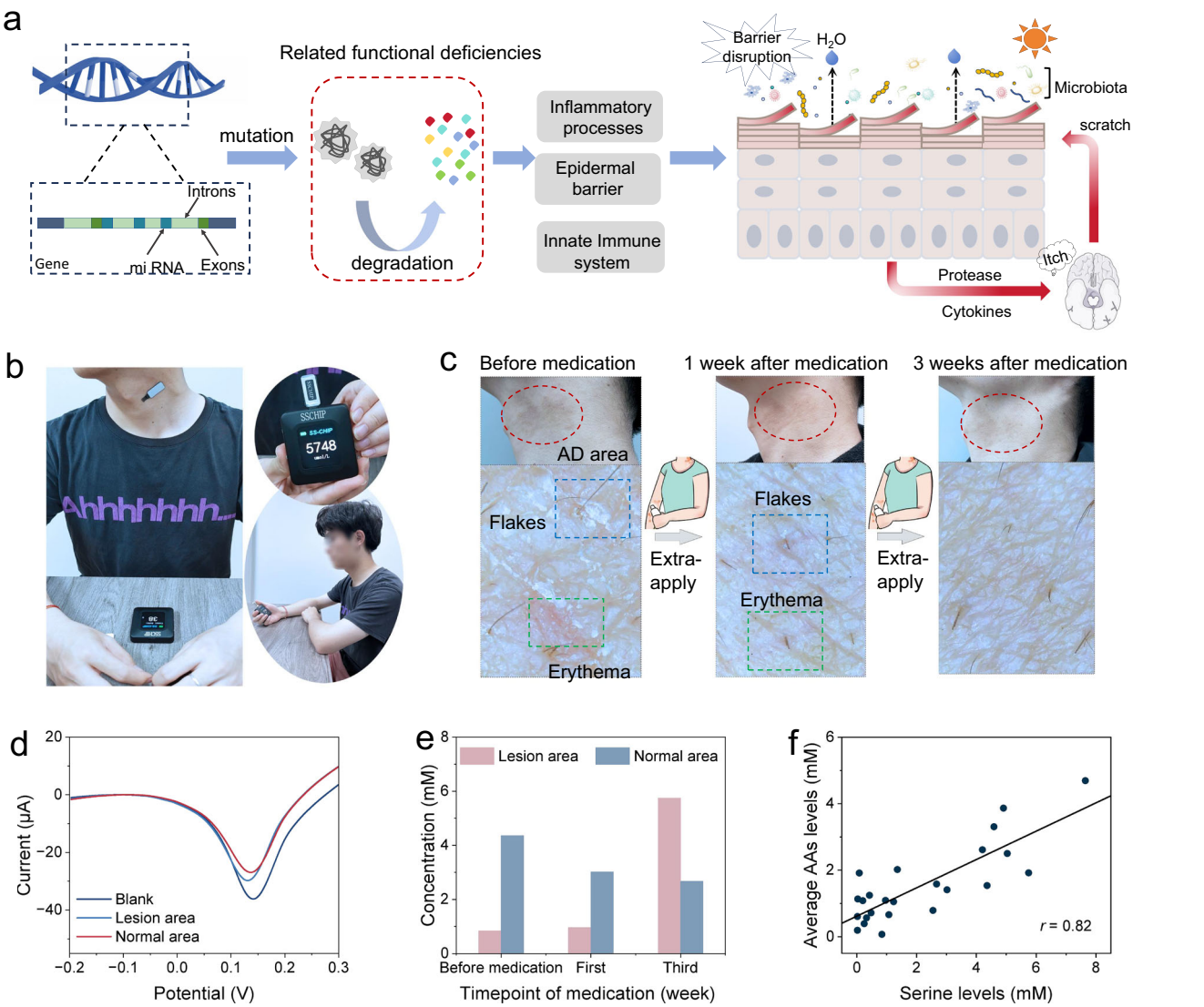

Fig. 4 | Serine sensing System for tracking treatment of a patient with AD. **a** Filaggrin gene mutation in the pathogenesis of AD. **b** Photographs of the AD patient using the system to measure the epidermal serine level after his lesion skin area recovered. **c** Optical images and corresponding magnified photographs of lesion areas in the AD patient at different stages of treatment. Erythema and flakes are highlighted in these images. **d** Sensor-measured response currents in the lesion and normal areas. **e** Histogram of epidermal serine levels in the lesion and normal areas at different medication timepoints. **f** Epidermal serine levels measured by the system versus AAs obtained by a commercial colorimetric assay kit. The line represents the linear-fitted trendline.

results not only deepened the understanding of the role of serine in skin hydration function but also fully validated the effectiveness and reliability of the developed sensing system in evaluating cosmetic products for improving the stratum corneum moisturizing function.

System evaluation for tracking treatment of a patient with atopic dermatitis

Atopic dermatitis (AD) is a chronic inflammatory skin disease, the main triggering factor for its onset is the mutations in the filaggrin gene[53]. These mutations result in filaggrin functional deficiency, impeding the degradation process of filaggrin into NMFs with a large proportion of serine in the stratum corneum[54,55]. Consequently, skin hydration and barrier function are diminished, which renders the skin more susceptible to external aggressors (e.g., allergens, irritants) and leads to skin lesions, exacerbating AD symptoms (Fig. 4a). Without the need for traditional clinical detection tools, in situ monitoring of biochemical indicators for skin diseases can offer a convenient method and a comprehensive molecular-level insight beyond existing portable or wearable techniques used to characterize of the skin physical properties[56–58].

Given the intimate connection between serine levels and the pathophysiology of AD, we employed the serine sensing system to quantitatively monitor epidermal serine levels in neck lesions and healthy skin areas on a patient diagnosed with AD (Fig. 4b and Supplementary Movie 2). Serine levels in the lesion skin during the recovery process were also tracked after receiving a topical prescription (0.1% tacrolimus ointment) treatment under medical supervision. Moreover, since optical imaging can provide visualized morphological information[59], a camera, and a handheld optical microscope were used to record the morphology and characteristics of the lesion skin during medication (Fig. 4c). In this process, we delved into the relationship between serine level fluctuations and the repair progress of the skin barrier function.

Before medication, the peak current response measured by our system in the lesion skin area was higher than that of the normal skin area (Fig. 4d), which reveals the decrease in epidermal serine levels due to the impaired skin barrier. With the intervention and treatment of topical medication, we observed a gradual increase in epidermal serine levels in the lesion area, corresponding to the improvement and repair

of the skin barrier function after medication (Fig. 4e). Specifically, after one week of medication, the epidermal serine level in the lesion area increased but remained lower than that in the normal area, suggesting that further topical medication was needed for treatment. In the third week after medication, the epidermal serine level in the lesion area significantly increased and even surpassed that in the normal area, which indicates that the skin barrier function in the lesion area had recovered to the normal state. Importantly, corresponding optical images and TEWLs at different medication time points also visually illustrate the recovery process and the therapeutic effect (Fig. 4c and Supplementary Fig. 28). In the optical images, the lesion skin area shows a dry and inflamed clinical appearance with evident erythema and flakes. The TEWL values on the lesion skin are significantly higher than those on the normal adjacent skin prior to medication, indicating severe impairment of the skin barrier function and substantial water loss. One week after topical medication, the erythema and flakes on the skin gradually subsided, and the skin barrier function is in the process of gradual recovery. Correspondingly, TEWL values remain relatively high but have decreased compared to pre-treatment level. Three weeks after topical medication, the appearance of the original lesion skin area recovered to the same as the normal area. TEWL values of the lesion skin area are also comparable to those of normal areas. This indicates that the skin barrier function had been effectively repaired and basically returned to normal. The normal area adjacent to the lesion area shows no significant changes in TEWL values during the whole process, but these TEWL values are still slightly higher than those on the normal skin of healthy individuals. Those improvements in skin barrier function align with the rising trend in epidermal serine levels, which implies that serine serves as a potential biomarker to assess the progress of recovery from AD.

Notably, the previous results of epidermal serine levels measured by our system show a strong correlation with the average amino acid levels obtained by a commercial colorimetric assay kit in the respective sampled hydrogels (Fig. 4f). As expected, we can reliably analyze the corresponding NMF levels based on the measured epidermal amino acid levels because the main components of NMF are amino acids, whose main component is serine.

Discussion

We have developed a serine sensing system integrated with a wearable serine sensing patch and a customized handheld tester for the in-situ sampling and measurement of epidermal serine levels. The disposable and low-cost patch consists of a porous hydrogel for serine diffusion and ion conduction, an electrochemical electrode array for indirect detection of serine within the hydrogel matrix, and a series of encapsulation layers. The portable serine tester is designed to insert the patch after serine sampling for real-time electrochemical measurement and result readout. The integrated system offers the advantages of ease of use and acceptance due to its simple and efficient operation steps, which is comparable to commercial glucose meters. As such, we anticipate that it has the potential to be widely used by dermatologists and even the general public for practical applications related to skin healthcare.

To evaluate its practical application value for skin healthcare, we demonstrated the capability of our system for assessing the cosmetic moisturizing efficacy and tracking the treatment and recovery process of an AD patient by in situ and real-time monitoring of the changes in epidermal serine levels. The utility of our system makes skin health monitoring less cumbersome and more acceptable to users and patients by eliminating the need for frequent hospital visits and complex testing procedures. To the best of our knowledge, few related systems have been reported for the detection of epidermal biomarkers and their applications in skin healthcare. More importantly, the system architecture and methodology proposed in this article are universal and scalable for the in situ and real-time detection of other water-soluble small molecules in the epidermis, which are associated with a vast range of important skin disorders and conditions in dermatology and cosmetics.

Methods

Materials

All chemical reagents were purchased from InnoChem (China) unless otherwise stated.

Preparation of the serine sensor

Initially, the carbon ink (Jujo Printing Supplies & Technology, Japan) was spin-coated onto a clean polyethylene terephthalate (PET) with a thickness of 0.08 mm (Huanan Xiangcheng Technology, China) as the substrate layer. The spin-coating process was conducted twice at 3000 rpm for 15 s with an acceleration rate of 200 rpm/s. After drying, the prepared carbon electrode was cut into the pre-designed shape using a laser cutting machine (Suzhou Inngu Laser, China). The carbon electrode was then activated by cyclic voltammetry (CV) scanning in 0.5 M H_2SO_4 (Fengchuan, China) for 60 segments, ranging from −1.2 to 1 V at a scan rate of 500 mV/s. The activated carbon electrode was further modified with electrochemically synthesized PBNPs as the active layer by CV scanning in a mixed solution containing 3 mM $FeCl_3$, 3 mM $K_3Fe(CN)_6$, 0.1 M HCl (Fengchuan, China), and 0.1 M KCl for 20 cycles (from −0.2 to 0.6 V at a scan rate of 50 mV/s). This process was repeated three times to ensure stable and optimal redox signals. As such, the sensor would exhibit a stable 115 μA LSV current peak in 0.1 M KCl. After that, the electrode was rinsed with distilled water and immersed in a solution comprising 0.1 M HCl and 0.1 M KCl for repeated CV scans (from −0.2 to 0.6 V at a scan rate of 50 mV/s) until a stable response was achieved for the PBNPs layer.

The preparation process of the MIP layer was carried out in a 0.1 M PBS solution containing 5 mM serine, 12.5 mM APBA, and 37.5 mM pyrrole. The MIP layer was electrochemically synthesized on the electrode via CV deposition (0–1 V, 5 cycles, 50 mV/s). The electrode was then soaked in an acetic acid/methanol mixture (7:3 v/v) for 12 h to extract the serine molecules. Following this, the prepared MIP-based electrode was immersed in 0.1 M KCl and conducted CV scans (from −0.2 V to 0.6 V at a scan rate of 50 mV/s) until a stable response was achieved. For the preparation of the NIP-based electrode, the same procedure was followed, with the exception that no template was added to the polymerization solution.

To fabricate the Ag/AgCl reference electrode, a silver layer was deposited on the substrate electrode surface using a multi-current steps technology in an electrolyte solution composed of 0.25 M silver nitrate, 0.75 M sodium thiosulfate, and 0.5 M sodium bisulfite. The electrochemical deposition parameters are as follows: −0.01 mA for 150 s, −0.02 mA for 50 s, −0.05 mA for 50 s, −0.08 mA for 50 s, and −0.1 mA for 350 s. Subsequently, 0.1 M $FeCl_3$ solution was dripped onto the Ag surface for 20 s, and then immediately rinsed distilled water. A cocktail for reference potential stabilization was then drop-coated onto the Ag/AgCl electrode surface (3 μL), which was a mixture of 250 mg NaCl, 395.5 mg 79.1 mg polyvinyl butyral (PVB), 10 mg Poly (ethylene glycol)-block-poly(propylene glycol)-block-poly(ethylene glycol) (F127, purchased from Sigma-Aldrich, USA), and 1 mg MWCNTs (XFNANO Materials, China) dispersed uniformly in 5 mL methanol.

Preparation of the porous PVA hydrogel

Initially, PVA (Mw ≈ 89,000, purchased from Sigma-Aldrich, USA) was dissolved in water at a weight ratio of 1:10 and heated at 90 °C for 2 h to obtain a homogeneous and transparent PVA solution. Separately, KOH was dissolved in water at a weight ratio of 1:5. Under continuous stirring, 14 g KOH solution was gradually added dropwise to 10 g PVA solution, and then 2.6 g of sucrose was dissolved into this mixture to form the precursor solution for the hydrogel. Next, 15 g precursor solution was poured into a petri dish (9 cm in diameter) and placed in a

vacuum desiccator to remove excess water and facilitate cross-linking. The hydrogel was then immersed in deionized water to eliminate the sucrose template and excess KOH until it reached a neutral pH. Following this, the porous PVA hydrogel was cut into a desired shape and stored in 0.1 M KCl solution for subsequent use.

Characterization of the serine sensor

All in vitro characterizations of prepared sensors were performed through an electrochemical workstation (CHI760E) in the solution of 0.1 M KCl or the PVA hydrogel containing 30 μL. For the MIP-based serine sensor, LSV analysis was performed across varying concentrations of serine. The LSV parameters were set as follows: sweep voltage from −0.2 to 0.4 V, scan rate of 50 mV/s, quiet time of 2 s, and sensitivity of 1×10^{-4} A/V. Prior to each LSV scan, an incubation period of 5 minutes was conducted to ensure that the sensor reached the quasi-steady state. The selectivity testing for the serine sensor was performed in a series of common interferent species solutions (3 mM serine, 0.06 mM Phe, 0.16 mM Tyr, 0.16 mM Glu, 1.2 mM Gly, 0.8 mM His, 1.8 mM urea, 4.5 mM lactic acid, 0.5 mM uric acid).

The surface morphology of the aforementioned electrodes in different preparation steps was characterized by Field Emission Scanning Electron Microscopy (FSEM, Hitachi SU8020, Japan), including the carbon electrode, the MIP-based electrode before and after template removal, as well as the NIP electrode before and after template removal.

Fabrication and assembly of the serine sensing patch

The laser-cutting device was employed to process the sensing chamber and two encapsulation layers of the sensor. All laser-engraved patterns were pre-designed using AutoCAD 2020. Specifically, a waterproof tape was cut into rounded rectangles of appropriate size as the encapsulation layer for the upper and lower layers to effectively inhibit water loss in the hydrogel. a chamber for placing the hydrogel was penetrated with a through-hole (diameter = 0.95 mm, thickness = 0.32 mm) in a double-side tape. All layers were vertically assembled, from top to bottom, which was the top encapsulation layer, the sensing chamber, the serine sensing electrode, and the bottom encapsulation layer. The top encapsulation layer can be torn off and attach the patch to the skin when used.

Circuit design of the handheld serine tester

The circuit module of the serine sensing tester comprises four primary parts: First, the microcontroller unit (MCU) serves as the core control unit of the tester system. Second, the power management system ensures a stable power supply. Finally, the three-electrode circuit and the screen control circuit are respectively responsible for specific signal processing and display control functions. Through precise connection and configuration, all components collaborate seamlessly to achieve LSV potential waveform signal readout, processing, transmission, and display.

As the core of the MCU control circuit, an STM32F301K8U6 chip is capable of delivering high-performance digital signal processing and meeting the demands of multiple peripheral interfaces. For LSV scanning, a predefined excitation potential waveform was applied across the working electrode and the reference electrode through a 12-bit digital-to-analog converter (DAC) built in MCU. The resulting current signals were then converted into voltage signals by a transimpedance amplifier within the circuit. Then these converted voltage signals were captured by an integrated 12-bit Analog-to-Digital Converter (ADC) built in the MCU, constructing a relationship curve between the excitation voltage and current signals. The MCU performed baseline correction, filtering, and smoothing on the raw LSV data. By utilizing the measured LSV curve in the blank solution (0.1 M KCl) as a calibration standard, subsequent LSV curves of serine levels were calibrated. Based on the calibrated data and a preset algorithm, the MCU converted the processed data into serine concentration values.

The MCU transmitted the epidermal serine level result to a liquid crystal display (LCD) screen through a high-speed serial peripheral interface (SPI) protocol. The screen is a 1.83-inch IPS color LCD screen with a power supply voltage of 3.3 V and a resolution of 240 x 280. It is driven by a NV3030B chip to ensure clear display content and bright colors.

The power management system is divided into a regulated power supply circuit and a charging management circuit. The regulated power supply module uses a rechargeable 3.7 V lithium-ion polymer battery with appropriate capacity and size as the main power supply. The battery voltage was converted into stable 3.3 V digital and analog power supplies through a low dropout linear regulator (662 K) to reduce potential interference from digital circuits on analog signals. The core of the charging management circuit is a power management chip (4056 A), which uses the power transistors inside the chip to perform constant current and constant voltage charging on the battery.

Program design of the handheld serine tester

The software component was designed in accordance with the functional modules of the hardware circuitry, utilizing the Keil μVision 5 integrated development environment and the C programming language for software editing, compilation, and real-time debugging. The system's relevant programs encompass a MAIN program, an A/D conversion subroutine, a D/A conversion subroutine, a data processing subroutine, and an LCD display driver subroutine. The programs developed on the personal computer were written into the MCU by the ST-Link. The MCU was connected to the ST-Link through pins including power, ground, clock, and data lines (VCC, GND, SWCLK, SWDIO). The ST-Link was configured as the debugger in the Keil μVision 5, and the designed program was burned into the Flash memory of the MCU.

Shell design of the handheld serine tester

The shell of the tester was designed by Solidworks and made by machining, which includes an upper cover plate and a bottom back plate. Screw fixing points were reserved around the plates for fixing each other. A charging port, a button port, a sliding switch interface, and a patch socket were reserved on the shell. In addition, the hollow area in the middle of the upper cover plate could place the LCD display screen. The whole tester's shell was elaborately designed to ensure a suitable layout of internal components while maintains the overall compactness and portability, which is convenient for users to carry and use. This customized shell is fully parameterized, allowing for easy scaling and adjustment of tolerances according to user needs to achieve optimal fit.

Ethics

The human subject experiments strictly adhere to the ethical guidelines set forth by institutional or national research committees, as well as the Declaration of Helsinki of the World Medical Association. This particular study has received ethical approval from the Human Study Ethics Committee of Beijing Forestry University (Approval No. BJFUPSY-2024-049). All participants aged between 22 and 27 were recruited through verbal recruitments. Each participant was paid between 50 to 200 RMB (depending on the participation time) as the compensation for the test. Prior to testing, all participants provided written informed consent. The recruited subjects comprised seven healthy individuals and one patient with atopic dermatitis (AD). Furthermore, the seven healthy subjects recruited reported no history of allergies and presented with no skin lesion on the inner side of the forearm. The patient with AD, whose affected area on the neck does not exhibit severe erosion, exudation, or secondary infection.

Serine sensing system validation on human subjects

To validate the feasibility of our serine sensing system for detecting skin serine levels and analyzing skin conditions, we selected the inner side of subject's forearm as the sampling site, the baseline characteristics of participants are detailed in Supplementary Table 3. The entire test was conducted in a relatively closed laboratory environment. During the experiment, the temperature was precisely controlled between 25 ± 1 °C, and the relative humidity was stably maintained within the range of 50 ± 5%. Considering the experiment primarily focuses on the short-term effect of a skincare product, we did not impose extremely strict restrictions on the specific time points for sampling within a day. Before participating in the test, subjects were strictly prohibited from using moisturizing, exfoliating, acid-containing, or other products that may affect the metabolism of the skin's stratum corneum and the serine level in the test area within 12 h. In order to obtain the original surface information and serine level of the stratum corneum, no pre-treatment of the skin was required to prevent any mechanical of chemical damage to the stratum corneum and destruction of the skin surface metabolite components.

Before measurement, subjects were asked to sit quietly and rest for 30 minutes under the set environmental conditions to allow the skin to fully adapt to the environment and stabilize its baseline state. Then, subjects used the portable serine sensing system to measure serine levels in the various skin states in this work according to the operating instructions provided by us. A disposable patch was provided for each measurement.

When studying the robustness of the serine sensing system, we selected the forehead, the back of the hand, and the inner side of the forearm as the sampling sites. For tracking the treatment progress of the AD patient (three weeks), we chose the lesion area on the patient's neck and the normal skin area surrounding the lesion as the test sites, the baseline characteristics of the patient are detailed in Supplementary Table 4. For the lesion area, obvious erythema and flakes were observed. The normal skin area surrounding the lesion was selected within a range of 2–3 cm from the edge of the lesion. A series of measurements were conducted during topical medication (at the 1st week and 3rd week) on both the lesion skin and adjacent normal skin areas. The specific timepoint for test was in the afternoon, and the method is the same as mentioned above, including environmental temperature and humidity control, skin treatment, and operational procedures. During this process, the improvement in the appearance of the lesion skin was recorded and photographed. All epidermal serine measurements using the serine sensing system were completed by the subjects themselves according to the operating instructions.

Colorimetry for system verification

All hydrogels within the patches after the previous measurements were collected and dried in 1.5 mL centrifuge tubes, and then stored at −25 °C. These hydrogels were further used to measure the average serine levels and the average AAs levels in their matrixes using the corresponding colorimetric assay kits. In order to extract serine/AAs from the hydrogels, dry hydrogel samples were immersed in 200 μL deionized water for 12 h to ensure that serine/AAs in hydrogel can be fully dissolved in water. The above extracts were directly used for subsequent colorimetric analysis. the L-Serine ELISA Kit (Immusmol, France) and the AAs assay kit (Solarbio, China) were used by following the steps on their instructions for the determinations of serine and AAs levels in the hydrogels, respectively.

The sampling of epidermal serine in the stratum corneum was conducted using a 3 M tape (Scotch book tape) cut to a 9 mm diameter. Initially, the tape was carefully placed on the skin surface without applying any additional pressure. A 100 g weight was then placed on the tape and maintained for 1 minute to ensure thorough adhesion and sampling. After the tape was smoothly peeled from the skin, the peeled tape was placed into a pre-labeled 1.5 mL centrifuge tube immediately and then stored at −25 °C. The collected tapes were further used to measure the serine levels using the colorimetric assay kits. Before colorimetric measurement, the tape was immersed in 200 μL of deionized water and subjected to 30 min of ultrasonic treatment to effectively extract the water-soluble serine molecules. The extracts were directly used for subsequent colorimetric analysis using the L-Serine ELISA Kit for the determination of serine and AAs levels in the tapes.

Statistical analysis

Statistical analyses were conducted using SPSS version 25 (IBM, USA) and Origin version 2024 (OriginLab, USA). We employed the least squares method of linear regression to establish the linear relationship between variables, which allowed us to calculate the Pearson correlation coefficient (r). Additionally, we used a two-tailed paired t-test to determine the statistical difference in epidermal serine levels before and after the application of essence. The result showed a statistically significant difference with a P-value of 0.003 ($^*P < 0.05$). Prior to conducting the t-test, we assessed the normality of the data using the Shapiro-Wilk test to ensure the validity of our t-test. The result indicated that the data met the assumption of normality with a P-value of 0.338 ($P > 0.05$).

Reporting summary

Further information on research design is available in the Nature Portfolio Reporting Summary linked to this article.

Data availability

All data supporting the findings of this study are available within the article and its supplementary files. Any additional requests for information can be directed to, and will be fulfilled by, the corresponding authors. Source data are provided with this paper (https://figshare.com/s/f8bb1464fd0f746e0782). Source data are provided in this paper.

Code availability

The codes used for simulation and data measurement are available from the corresponding authors upon reasonable request.

References

1. Min, J. et al. Skin-interfaced wearable sweat sensors for precision medicine. *Chem. Rev.* **123**, 50495138 (2023).
2. Qin, X. et al. Manufacturing high-performance flexible sensors via advanced patterning techniques. *Int. J. Extrem. Manuf.* **7**, 032003 (2025).
3. Zhong, B. et al. A crosstalk-free dual-mode sweat sensing system for naked-eye sweat loss quantification via changes in structural reflectance. *Bio-Des. Manuf.* **7**, 428–438 (2024).
4. Li, Z., Chen, F., Zhu, N., Zhang, L. & Xie, Z. Tip-enhanced sub-femtomolar steroid immunosensing via micropyramidal flexible conducting polymer electrodes for at-home monitoring of salivary sex hormones. *ACS Nano* **17**, 21935–21946 (2023).
5. Lu, X. et al. Framework nucleic acids combined with 3D hybridization chain reaction amplifiers for monitoring multiple human tear cytokines. *Adv. Mater.* **36**, 2400622 (2024).
6. Ausri, I. R. et al. Multifunctional dopamine-based hydrogel microneedle electrode for continuous ketone sensing. *Adv. Mater.* **36**, 2402009 (2024).
7. Yang, Y. et al. A laser-engraved wearable sensor for sensitive detection of uric acid and tyrosine in sweat. *Nat. Biotechnol.* **38**, 217–224 (2020).
8. Xu, C. et al. A physicochemical-sensing electronic skin for stress response monitoring. *Nat. Electron.* **7**, 168–179 (2024).
9. Cai, X. et al. Fully integrated multiplexed wristwatch for real-time monitoring of electrolyte ions in sweat. *ACS Nano* **18**, 12808–12819 (2024).

10. Tu, J. et al. A wireless patch for the monitoring of c-reactive protein in sweat. *Nat. Biomed. Eng.* **7**, 1293–1306 (2023).
11. Ye, C. et al. A wearable aptamer nanobiosensor for non-invasive female hormone monitoring. *Nat. Nanotechnol.* **19**, 330–337 (2024).
12. Gao, F. et al. Wearable and flexible electrochemical sensors for sweat analysis: a review. *Microsyst. Nanoeng.* **9**, 1 (2023).
13. Yang, Y. & Gao, W. Wearable and flexible electronics for continuous molecular monitoring. *Chem. Soc. Rev.* **48**, 1465–1491 (2019).
14. Davis, N., Heikenfeld, J., Milla, C. & Javey, A. The challenges and promise of sweat sensing. *Nat. Biotechnol.* **42**, 860–871 (2024).
15. Bakshi, P., Vora, D., Hemmady, K. & Banga, A. K. Iontophoretic skin delivery systems: success and failures. *Int. J. Pharm.* **586**, 119584 (2020).
16. Saha, T., Del, C. R., De la Paz, E., Sandhu, S. S. & Wang, J. Access and management of sweat for non-invasive biomarker monitoring: a comprehensive review. *Small* **19**, e2206064 (2023).
17. Zhong, B., Jiang, K., Wang, L. & Shen, G. Wearable sweat loss measuring devices: from the role of sweat loss to advanced mechanisms and designs. *Adv. Sci.* **9**, 2103257 (2022).
18. Xu, Y. et al. In-ear integrated sensor array for the continuous monitoring of brain activity and of lactate in sweat. *Nat. Biomed. Eng.* **7**, 1307–1320 (2023).
19. Moon, J. M. et al. Non-invasive sweat-based tracking of L-dopa pharmacokinetic profiles following an oral tablet administration. *Angew. Chem. Int. Ed.* **60**, 19074–19078 (2021).
20. Stoffers, K. M., Cronkright, A. A., Huggins, G. S. & Baleja, J. D. Noninvasive epidermal metabolite profiling. *Anal. Chem.* **92**, 12467–12472 (2020).
21. Montano, E., Bhatia, N. & Ostojić, J. Biomarkers in cutaneous keratinocyte carcinomas. *Dermatol. Ther.* **14**, 2039–2058 (2024).
22. Jankovskaja, S. et al. Non-invasive, topical sampling of potential, low-molecular weight, skin cancer biomarkers: a study on healthy volunteers. *Anal. Chem.* **94**, 5856–5865 (2022).
23. Lyubchenko, T., Collins, H. K., Goleva, E. & Leung, D. Y. M. Skin tape sampling technique identifies proinflammatory cytokines in atopic dermatitis skin. *Ann. Allerg. Asthma Im.* **126**, 46–53 (2021).
24. Wang, C. Y. & Maibach, H. I. Why minimally invasive skin sampling techniques? A bright scientific future. *Cutan. Ocul. Toxicol.* **30**, 1–6 (2011).
25. Fritz, B. et al. RNA-sequencing of paired tape-strips and skin biopsies in atopic dermatitis reveals key differences. *Allergy* **79**, 1548–1559 (2024).
26. Ratley, G. et al. The circadian metabolome of atopic dermatitis. *J. Allergy Clin. Immun.* **153**, 1148–1154 (2024).
27. Vander Pyl, C., Feeney, W., Arroyo, L. & Trejos, T. Capabilities and limitations of GC-MS and LC-MS/MSC for trace detection of organic gunshot residues from skin specimens. *Forensic Chem.* **33**, 100471 (2023).
28. Grégoire, S. et al. Hyaluronic acid skin penetration evaluated by tape stripping using elisa kit assay. *J. Pharm. Biomed.* **224**, 115205 (2023).
29. Rawlings, A. V. & Harding, C. R. Moisturization and skin barrier function. *Dermatol. Ther.* **17**, 43–48 (2004).
30. Arezki, N. R., Williams, A. C., Cobb, A. J. A. & Brown, M. B. Design, synthesis and characterization of linear unnatural amino acids for skin moisturization. *Int. J. Cosmet. Sci.* **39**, 72–82 (2017).
31. Cork, M. J. et al. Epidermal barrier dysfunction in atopic dermatitis. *J. Invest. Dermatol.* **129**, 1892–1908 (2009).
32. Nouwen, A. E. M. et al. Natural moisturizing factor as a clinical marker in atopic dermatitis. *Allergy* **75**, 188–190 (2020).
33. Maeno, K. Direct quantification of natural moisturizing factors in stratum corneum using direct analysis in real time mass spectrometry with inkjet-printing technique. *Sci. Rep.* **9**, 17789 (2019).
34. Kim, H. et al. Combined skin moisturization of liposomal serine incorporated in hydrogels prepared with carbopol ETD 2020, rhesperse RM 100 and hyaluronic acid. *Korean J. Physiol. Pharmacol.* **19**, 543–547 (2015).
35. Takeichi, T. et al. Reduction of stratum corneum ceramides in Neu-Laxova syndrome caused by phosphoglycerate dehydrogenase deficiency. *J. Lipid Res.* **59**, 2413–2420 (2018).
36. Handzlik, M. K. & Metallo, C. M. Sources and sinks of serine in nutrition, health, and disease. *Annu. Rev. Nutr.* **43**, 123–151 (2023).
37. Kim, J. et al. Amino acids disrupt calcium-dependent adhesion of stratum corneum. *PLoS One* **14**, e215244 (2019).
38. Xiong, Q. et al. LC-MS metabolomics reveal skin metabolic signature of psoriasis vulgaris. *Exp. Dermatol.* **32**, 889–899 (2023).
39. Yoshihisa, Y. et al. Inflammatory cytokine-mediated induction of serine racemase in atopic dermatitis. *J. Cell. Mol. Med.* **22**, 3133–3138 (2018).
40. Kamleh, M. A. et al. LC–MS metabolomics of psoriasis patients reveals disease severity-dependent increases in circulating amino acids that are ameliorated by anti-TNFα treatment. *J. Proteome Res.* **14**, 557–566 (2015).
41. Mlitz, V. et al. Impact of filaggrin mutations on Raman spectra and biophysical properties of the stratum corneum in mild to moderate atopic dermatitis. *J. Eur. Acad. Dermatol. Venereol.* **26**, 983–990 (2012).
42. Amin, R., Lechner, A., Vogt, A., Blume-Peytavi, U. & Kottner, J. Molecular characterization of xerosis cutis: a systematic review. *PLoS One* **16**, e261253 (2021).
43. Wu, D. et al. A comprehensive review on signaling attributes of serine and serine metabolism in health and disease. *Int. J. Biol. Macromol.* **260**, 129607 (2024).
44. He, L., Ding, Y., Zhou, X., Li, T. & Yin, Y. Serine signaling governs metabolic homeostasis and health. *Trends Endocrinol. Met.* **34**, 361–372 (2023).
45. Tang, W. et al. Touch-based stressless cortisol sensing. *Adv. Mater.* **33**, 2008465 (2021).
46. Mukasa, D. et al. A computationally assisted approach for designing wearable biosensors toward non-invasive personalized molecular analysis. *Adv. Mater.* **35**, 2212161 (2023).
47. Zhong, B. et al. Interindividual- and blood-correlated sweat phenylalanine multimodal analytical biochips for tracking exercise metabolism. *Nat. Commun.* **15**, 624 (2024).
48. Wang, M. et al. A wearable electrochemical biosensor for the monitoring of metabolites and nutrients. *Nat. Biomed. Eng.* **6**, 1225–1235 (2022).
49. Engebretsen, K. A. et al. Effect of atopic skin stressors on natural moisturizing factors and cytokines in healthy adult epidermis. *Brit. J. Dermatol.* **179**, 679–688 (2018).
50. Piquero-Casals, J. et al. Urea in dermatology: a review of its emollient, moisturizing, keratolytic, skin barrier enhancing and antimicrobial properties. *Dermatol. Ther.* **11**, 1905–1915 (2021).
51. Stettler, H. et al. A new topical panthenol-containing emollient: results from two randomized controlled studies assessing its skin moisturization and barrier restoration potential, and the effect on skin microflora. *J. Dermatol. Treat.* **28**, 173–180 (2017).
52. Westermann, T. V. A. et al. Measurement of skin hydration with a portable device (skinup® beauty device) and comparison with the corneometer®. *Ski. Res. Technol.* **26**, 571–576 (2020).
53. Rerknimitr, P., Otsuka, A., Nakashima, C. & Kabashima, K. Skin barrier function and atopic dermatitis. *Curr. Dermatol. Rep.* **7**, 209–220 (2018).
54. Kezic, S. et al. Loss-of-function mutations in the filaggrin gene lead to reduced level of natural moisturizing factor in the stratum corneum. *J. Invest. Dermatol.* **128**, 2117–2119 (2008).

55. Kezic, S. et al. Levels of filaggrin degradation products are influenced by both filaggrin genotype and atopic dermatitis severity. *Allergy* **66**, 934–940 (2011).
56. Liu, Y. et al. Skin-interfaced superhydrophobic insensible sweat sensors for evaluating body thermoregulation and skin barrier functions. *ACS Nano* **17**, 5588–5599 (2023).
57. Madhvapathy, S. R. et al. Advanced thermal sensing techniques for characterizing the physical properties of skin. *Appl. Phys. Rev.* **9**, 041307 (2022).
58. Madhvapathy, S. R. et al. Reliable, low-cost, fully integrated hydration sensors for monitoring and diagnosis of inflammatory skin diseases in any environment. *Sci. Adv.* **6**, eabd7146 (2020).
59. Li, Z. et al. A reconfigurable heterostructure transistor array for monocular 3D parallax reconstruction. *Nat. Electron.* **8**, 46–55 (2025).

Acknowledgements

The authors sincerely acknowledge financial support from National Key Research and Development Program of China (Grant 2024YFB3212100), National Natural Science Foundation of China (NSFC Grant No. 62422409, 62174152, and 62374159), Open Fund of State Key Laboratory of Infrared Physics (grant no. SITP-NLIST-YB-2024-04), and the Youth Innovation Promotion Association of Chinese Academy of Sciences (No. 2020115).

Author contributions

Y.Y., B.Z., Z.L., and L.W. designed the research, Y.Y., B.Z., and L.W. wrote the paper, Y.Y., B.Z., X.Q., H.X., X.W., L.L., Z.X.L., Z.L., and L.W. performed the experiments, Y.Y., B.Z., L.L., W.Z., and Z.X.L. performed the simulations. Y.Y., B.Z., H.X., X.W., H.X., Z.L., and L.W. analyzed the data, Y.Y., B.Z., X.Q., and Y.F. designed the human studies. B.Z., Y.F., Z.L., and L.W. revised the paper, Z.L. and L.W supervised the project. All authors substantially contributed to research and reviewed the manuscript.

Competing interests

The authors declare the following competing interests: Y. Y., B. Z., H. X., Z. L., and L. W. are inventors of a patent related to this work (application no. ZL202410163381.9, CN). The other authors declare no competing interests.

Additional information

Supplementary information The online version contains supplementary material available at https://doi.org/10.1038/s41467-025-58147-0.

Correspondence and requests for materials should be addressed to Hao Xu, Zheng Lou, Yongming Fan or Lili Wang.

Peer review information *Nature Communications* thanks Carolina Pupe, and the other, anonymous, reviewer for their contribution to the peer review of this work. A peer review file is available.